Available online at www.sciencedirect.com
ScienceDirect
Acta Materialia 59 (2011) 3612–3620
Acta MATERIALIA
www.elsevier.com/locate/actamat

A method for in situ measurement of the elastic behavior of a columnar thermal barrier coating

C. Eberl [a,b,*], D.S. Gianola [a,c], X. Wang [a,d], M.Y. He [e], A.G. Evans [e], K.J. Hemker [a]

[a] Department of Mechanical Engineering, Johns Hopkins University, Baltimore, MD, USA
[b] Institute for Applied Materials, Karlsruhe Institute for Technology, Karlsruhe, Germany
[c] Department of Materials Science & Engineering, University of Pennsylvania, Philadelphia, PA, USA
[d] Institute of Mechanics, Chinese Academy of Science, Beijing, People's Republic of China
[e] Department of Materials, UCSB, Santa Barbara, CA, USA

Received 24 June 2010; received in revised form 16 February 2011; accepted 19 February 2011

Abstract

The mechanical behavior of a ceramic coating and the evolution of this behavior in-service play crucial roles in governing the performance and lifetime of these materials. A protocol is presented that allows for characterization of the in-plane elastic modulus and strain to failure of fragile ceramic coatings. The protocol employs digital image correlation (DIC) to measure time-resolved, full-field strain maps of bilayer microbeams, and material properties are extracted through direct comparison with finite element simulations of microbending experiments. The efficacy of the method is demonstrated by the measurement of the in-plane Young's modulus ($E_{TBC} = 15$–30 GPa) and the strain to fracture (3.5–5×10^{-3}) of electron beam physical vapor deposited 7% yttria-stabilized zirconia thermal barrier coatings (TBCs). The results from this study also indicate that the in-plane TBC modulus has no strain dependence when measured in tension.

Keywords: Thermal barrier coating (TBC); Digital image correlation; Elastic in plane modulus; Fracture strain; EB-PVD 7YSZ

1. Introduction

Thermal barrier coatings (TBCs) used on rotating components in modern aero-turbines are deposited onto single-crystal Ni-base superalloy airfoils (with intervening bond coat) by electron beam methods. This method allows precise control of the thickness of the layer and results in a columnar microstructure (Fig. 1), incorporating intercolumnar gaps and intracolumnar porosity. The former influences the compliance of the layer, while the latter affects its through-thickness thermal conductivity. The in-plane compliance limits the elastic energy, U_{el}, that can be stored in the layer because of its thermal expansion misfit with the substrate. The ensuing U_{el} is sufficiently small, relative to the toughness of the TBC, that it remains attached upon thermally cycling, enabling its application in turbines. The durability of the coating is strongly affected by U_{el} through the in-plane Young's modulus, E_{π}. However, direct measurements of this modulus are challenging and hence few have been reported. A fundamental difficulty is that removal of the coating from the substrate to make measurements causes it to fragment: its properties must be measured while still attached. Methods based on measurement of the acoustic wave velocity or of the vibration frequency can be used, but cannot be applied in situ to the TBC deposited on actual aerofoils. The purpose of the present article is to introduce a suitable test protocol for measuring the elastic response and strain to failure of an electron beam physical vapor deposited (EBPVD) TBC and to demonstrate its utility on a cylindrical config-

* Corresponding author at: Institute for Applied Materials, Karlsruhe Institute for Technology, Karlsruhe, Germany.
E-mail address: chris.eberl@kit.edu (C. Eberl).

1359-6454/$36.00 © 2011 Published by Elsevier Ltd. on behalf of Acta Materialia Inc.
doi:10.1016/j.actamat.2011.02.034

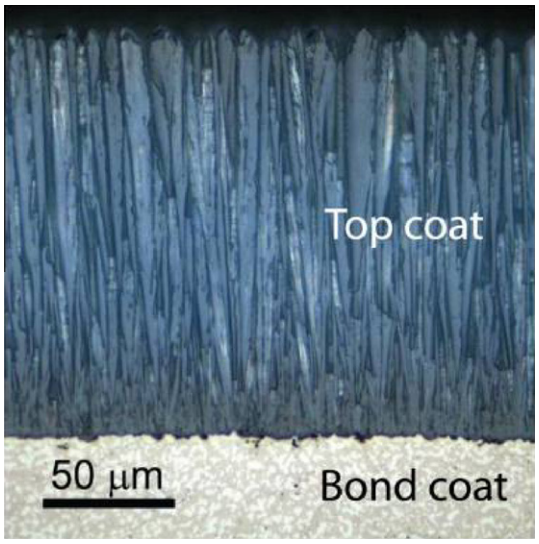

Fig. 1. The columnar microstructure commonly associated with an electron beam physical vapor deposited (EBPVD) 7% yttria-stabilized zirconia (7YSZ) thermal barrier coating (TBC).

uration known as the burner rig specimen, which is representative of that used for assessing thermal cycle durability [1].

The columnar structure produced during EBPVD reduces the in-plane Young's modulus, E_π of the TBC and imparts much needed TBC compliance. This columnar microstructure can and will vary with deposition parameters, substrate topology, and exposure to extreme temperatures and environments during service. Attendant changes in properties, namely the elastic properties, will play an important role in determining the performance and durability of the coating but are difficult to measure and remain to be elucidated. Moreover, microstructural variations across the thickness of the TBC could lead to a position-dependent modulus and the feathery nature of the columns have led some investigators to report that the in-plane modulus, E_π, depends on the imposed in-plane strain, ε_{xx} [2–4]. Here, the proposed microbending experiments are employed to characterize as-deposited coatings, but investigations involving microstructural evolution and other second-order effects are also practicable.

The paper is organized as follows. The measurement concept is described. The strain patterns constituting the basis for the in-plane Young's modulus E_π determinations are analyzed using the finite-element (FE) method and the preferred strain measurement locations identified. The strain results and their interpretation are presented, followed by a discussion of results and summary.

2. The measurement concept

The proposed measurement concept relies on microscale electrodischarge machining (EDM) to create an end-supported bilayer microbeam comprising the TBC coating and a thin section of the bond coat and/or substrate

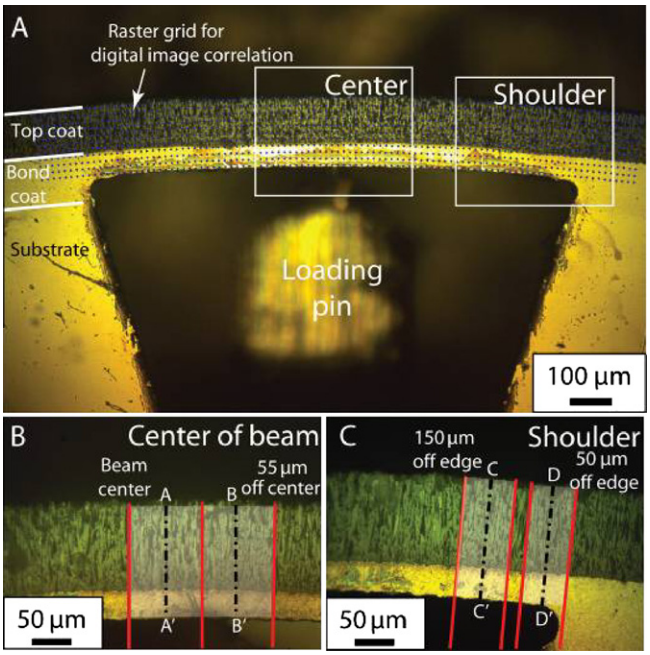

Fig. 2. (A) An optical image illustrating the test configuration and the microbeam sample geometry. Images of the (B) central and (C) shoulder regions of the microbeam. Strain (ε_{xx}) profiles were measured along paths BB′ (55 or 80 μm off-center) and CC′ (150 μm from the side).

(Fig. 2) [5]. To generate this configuration a cylindrical burner rig specimen is first sectioned to create a disc with the bond coat and TBC around the circumference of the disc. This is most readily achieved by utilizing the same mechanical methods developed for preparation of minimally damaged cross-sections for microscopic characterization of the TBC microstructure [6]. Thereafter, micro-EDM is used to remove a section of the underlying substrate while retaining the bilayer beam.

To introduce bending loads into the microbeam a microtensile testing set-up mounted on an air table is equipped with a steel load pin to pull from the inside at the center of the beam (Fig. 3). A fiv-axis piezo stage allows precise

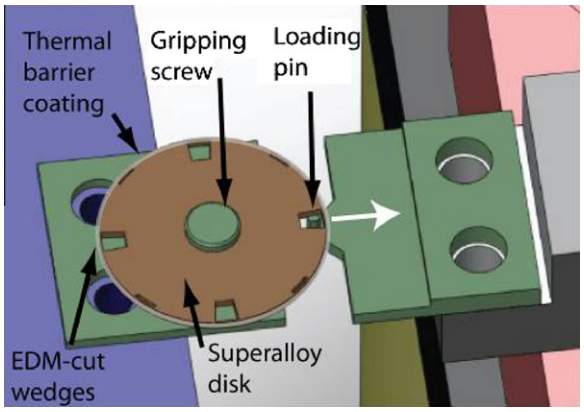

Fig. 3. Schematic of the microscale load frame devised for these experiments. The applied force is measured with an in-line load cell; full-field displacement maps are collected using a DIC routine and optical images obtained using a digital camera.

alignment of the load pin relative to the beam center and the load axis. The load can be measured by a load cell (load cells with 1 and 44.5 N capacity were used) and the full-field displacements and strains are tracked by an optical camera (Pixelink, PL-782) mounted on a standard optical microscope, which allows the field of view (FOV) to be changed from millimeters to hundreds of microns. Full-field displacement and strain data are extracted from a series of images by use of a digital image correlation (DIC) technique [7–9]. The DIC software suite developed at Johns Hopkins University utilizes Matlab (Mathworks) as the calculation engine and can be downloaded for free [10].

When loaded in this manner the TBC/bond coat bilayer contains a combination of bending and stretch (membrane) loads. Sufficiently long narrow beams and can be described with analytical solutions recently proposed by He et al. [11], but the geometry of the microbeams used in the current study limit the utility of these solutions. The response of the bilayer bridge has instead been analyzed by the FE method using the commercial code ABAQUS Standard. The FE mesh is depicted on Fig. 4a. The bond coat is considered to be elastic/plastic with power law hardening having the stress–strain relation presented elsewhere (yield strength, $\sigma_Y = 750$ MPa, isotropic Young's modulus, $E = 155$ GPa and strain hardening exponent, $n = 0.2$) [12]. In these simulations the TBC is parametrically assigned an in-plane modulus, E_{π}, in the range $10 \leqslant E_{\pi} \leqslant 50$ GPa, and the out-of-plane modulus (which has minimal effect on the strains) is considered to be $E_{\perp} \approx 160$ GPa (compared to $E_{solid} = 200$ GPa for dense YSZ).

A preliminary FE result calculated at a representative load and an intermediate choice for the in-plane TBC modulus reveals the strain pattern of the cross-section (Fig. 4b). Evidently, the strains are concentrated in the vicinity of the load line and exhibit rapid spatial variation in its vicinity. Similar but less pronounced spatial variability exists close to the supported ends. Consequently, the ensuing strain profiles were investigated at four positions, i.e. along the planes AA′, BB′, CC′ and DD′ (Fig. 2b and c) with the offset positions (BB′ 55 or 80 μm off-center; CC′ 150 μm from the shoulder) being preferable. The strains on these planes vary linearly with distance from the TBC surface. Consistent with beam theory, near the center the strains are predicted to be tensile near the top of the TBC, go through zero at the neutral axis, and become compressive in the bond coat. This trend is reversed near the shoulder, i.e. the strains are compressive at the top of the TBC, go through zero at the neutral axis, and become tensile in the bond coat.

Before proceeding with the numerical analysis, it is worth noting that the approximate magnitude of the in-plane Young's modulus of the coating can be ascertained from measurements of the location of the neutral axis h_0. That is, for a bilayer microbeam with TBC and bond coat of thickness h_1 and h_2, having (strain-invariant) in-plane Young's moduli, E_1 and E_2, respectively (the former being lower, i.e. the TBC), subject to a bending moment (no axial

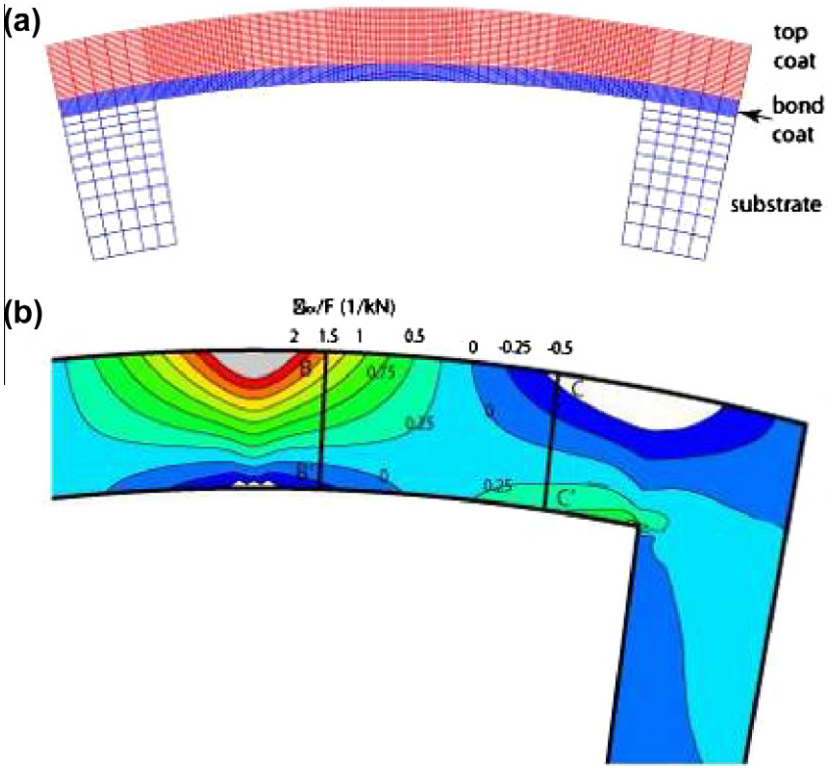

Fig. 4. (a) Finite element (FE) mesh used to simulate the elastic response of the TBC and the elastic–plastic response of the bond coat. (b) Predicted contours of normalized strain (ε_{xx}/F) calculated at a representative load level. The ε_{xx} strain varies linearly through the thickness of the TBC and is primarily tensile in the center of the microbeam and compressive near the shoulder.

force), the neutral axis is located at a distance from the tensile surface h_o, given by [13]:

$$\frac{h_o}{h_1} = \frac{1 + \frac{2E_2h_2}{E_1h_1} + \frac{E_2h_2^2}{E_1h_1^2}}{2\left(1 + \frac{E_2h_2}{E_1h_1}\right)} \quad (1)$$

Note that this location depends only on the thickness of the layers and their in-plane moduli (not on load). Thus, upon assuming that the axial force is relatively small (to be substantiated below), the unknown in-plane modulus of the TBC, E_{π}, can be estimated. This estimate may be used to establish a benchmark modulus. More precise values are determined from the numerical calculations, which account for the axial force as well as the strain dependence, starting with the benchmark as a trial value.

3. Experimental results

The cylindrical burner rig specimens, provided by Pratt & Whitney, contained 110 and 150 μm thick 7% yttrium-stabilized zirconia (7YSZ) coatings deposited by a EBPVD process onto nominally 130 μm thick low-pressure plasma-sprayed (LPPS) NiCoCrAlY bond coat. The underlying substrate for these samples was a Ni-base superalloy (PWA 1484). Cross-sections were sliced and polished from the cylindrical burner rig bars and high precision micro-EDM was used to remove a section of the substrate and part of the bond coat underneath the TBC coating. The final test geometry (Fig. 2a) consisted of a doubly-end-supported beam approximately 1 mm long. The supporting bond coat layer varied from specimen to specimen but was in the range of 35–65 μm, resulting in a bilayer microbeam that was a primarily TBC. The widths of the μbeams were 550 and 400 μm. Accordingly, the specimens have a relative span to thickness ratio, $L/h = 3$, coating to substrate thickness ratio, $h_1/h_2 = 3$, and in-plane modulus ratio, $E_2/E_1 \approx 6$.

The microbending experiment starts with mounting of the disc and alignment of the load pin and sample relative to the load axis, which is accomplished through a series of elastic loading cycles with very small maximum loads. Misalignment caused by eccentric loading or microscale surface roughness produces an easily identifiable hysteresis on the load–displacement curve and can be minimized by these repeated load/unload cycles. Digital image resolution is maximized by mounting the load frame on an optical air table that reduces vibrations, and by loading the sample in a stepwise fashion so that static images can be captured. The noise in the images is further reduced by using a short exposure time of approximately 40 ms and then averaging over 10 frames.

A dense full-field displacement map (with a raster size of 1 μm across a FOV of 400 μm × 290 μm) cannot be calculated in real time and requires post-processing. A coarse mesh is illustrated schematically in Fig. 2a, where[1] the blue dots correspond to possible marker positions that are identified and their motion tracked by the DIC routine. The actual mesh was an order of magnitude smaller than is illustrated here and the DIC tracking was done with sub-pixel resolution. This full-field displacement data can be used to calculate the local 2-D strain tensor at each point in the mesh. The theoretical DIC strain resolution is limited by the accuracy of the image data (e.g. color depth, resolution) but in practice it is limited by image noise and vibration. To achieve sufficient accuracy in the strain resolution, the displacement of a number of DIC raster points can be averaged. In the current study, the DIC raster points were averaged over an area of 5 μm × 50 μm to achieve a strain resolution of $d\varepsilon_{xx} = 2 \times 10^{-4}$. This allows us to acquire independent strain measurements every 5 μm along the y-axis with high resolution.

To maximize strain resolution, all experiments were conducted at 400× but the FOV is rather limited at this magnification and two separate experiments were conducted, focusing on either the center of the beam or a shoulder, while the microbeam is loaded in the center. Elastic displacements in the center of the microbeam were found to be large enough to measure the strain through the thickness of the bilayer microbeam, but the compressive strains in the shoulder were much smaller and hence difficult to track during purely elastic loading. However, at higher loads the TBC invariably cracked vertically near the center of the microbeam and the increased compliance associated with the presence of this crack greatly facilitated measurements of compressive strain in the shoulder regions. For this reason, both uncracked and cracked specimens were employed in the current study.

The in-plane strain (ε_{xx}) was measured as function of depth from the top of the TBC for a series of increasing loads, and representative curves are shown in Fig. 5. Curves taken 55 μm off-center (Fig. 5a) for this sample (TBC a–microbeam 1) show that the axial strain varied as predicted by elementary beam theory; the highest tensile strain was found at the surface of the top coat. Progressing through the top coat from the surface to the interface shows an almost linear decrease in strain. The strain crosses zero, delineating the neutral plane at a depth that is near the TBC–bond coat interface, and becomes negative in the bond coat.

The elastic strains in the shoulder regions of the microbeam (Fig. 5b) were smaller and harder to measure than the tensile strains in the center section. Efforts to measure the compressive strains with elastically loaded, fully intact coatings were inhibited by the magnitude of these strains and the fact that the TBC fails when loaded beyond a modest critical load. Above this load a vertical crack forms in the TBC, extending through the thickness and arresting at the bond coat–TBC interface. The crack forms above the point of loading near the center of the microbeam but the exact location is influenced by the distribution of flaws in the TBC. The critical strain to fracture in the TBC top coat was measured to be 3.5–5 × 10^{-3} for the

[1] For interpretation of color in Fig. 2, the reader is referred to the web version of this article.

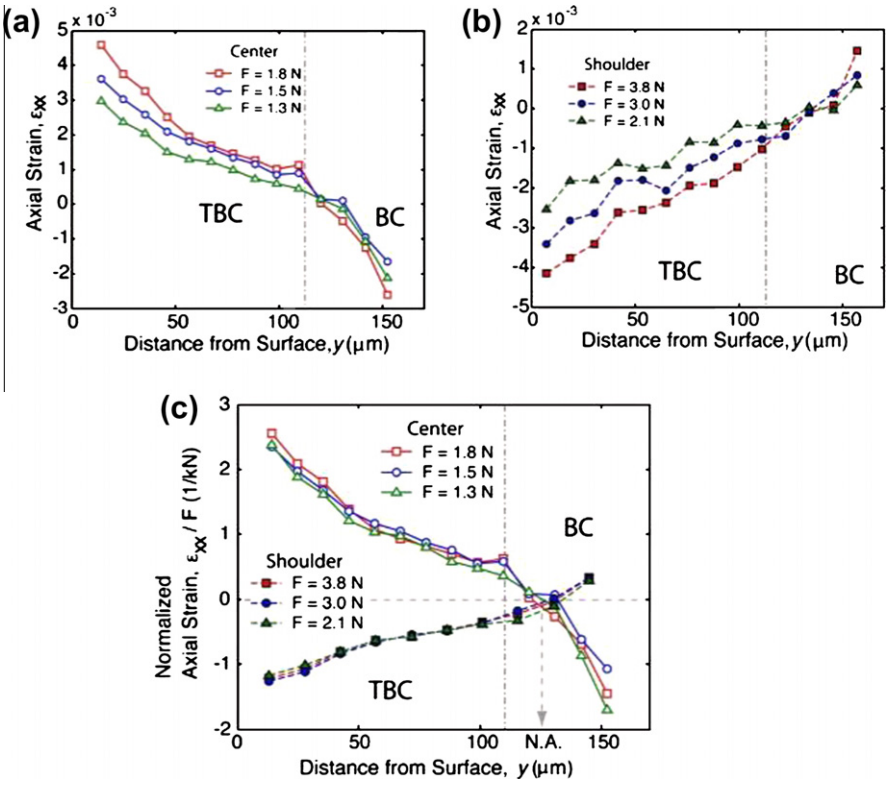

Fig. 5. Experimental measurements of strain (ε_{xx}) measured for three different loading conditions (a) near the center of the microbeam and (b) near the shoulder. Normalizing these curves by the applied force (c) collapses these data sets onto common curves for both the center and the shoulder region.

microbeams tested in this study. An example of the load response associated with crack nucleation is given in Fig. 6. The exact load at which the crack is nucleated can be identified by close inspection of the in situ images collected during loading, and the critical load for this sample was determined to be 2.0 N as illustrated by the change in compliance observed on the loading curve. The overall compliance of the microbeam was greatly increased by the presence of this vertical crack. This increased compliance and the ability to apply larger loads resulted in larger compressive strains in the shoulder section, which simplified their measurement (Fig. 5b). As expected, the ε_{xx} strain near the shoulder was compressive at the TBC surface, decreased with depth, and became tensile in the bond coat. The magnitude of the strain was observed to scale with applied load but was not sensitive to lateral position. The fact that the strain is less sensitive to position may be related to the presence of the crack, which acts as a hinge and results in more uniform loading away from the center point of the beam. This point was confirmed by FE simulations that incorporate the geometry of the specimen as well as the position and geometry of the TBC crack.

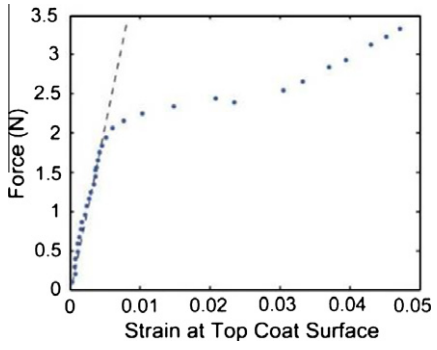

Fig. 6. Applied load vs. strain measured in the top center of the microbeam at the site of crack nucleation. The dashed line is a visual guide and the deviation of the measured strain from this line marks the deviation from linear elastic behavior (indicated by the dashed line). The deviation arises from with the introduction of a vertical crack in the TBC at a critical local strain of $\varepsilon_{xx} = 5 \times 10^{-3}$.

Plots of the ε_{xx} strain normalized by the applied force and plotted as a function of depth (Fig. 5c) show that the magnitude of the strain in the TBC scaled with applied load, while the neutral axis did not. The observation that the normalized data sets from the beam center and shoulder both collapse to universal curves indicates that the compliance of the microbeams measured in this study, and thus the in-plane modulus of the TBC, does not depend on strain as has previously been reported [2–4].

Experimental data for two additional specimens (TBC a–microbeam 2 and TBC b–microbeam 1) are given in Figs. 7 and 8, respectively. An estimate of the in-plane TBC modulus E_{π} based on Eq. (1), the positions of the neutral axes indicated in Figs. 5, 7 and 8, the dimensions of the bilayer microbeams and the isotropic bond coat modulus ($E_{bc} = 155$ GPa [12]) indicates that a reasonable benchmark for the in-plane modulus of the TBC is $E_{TBC} = 15$–25 GPa (see Table 1). The complex specimen geometry

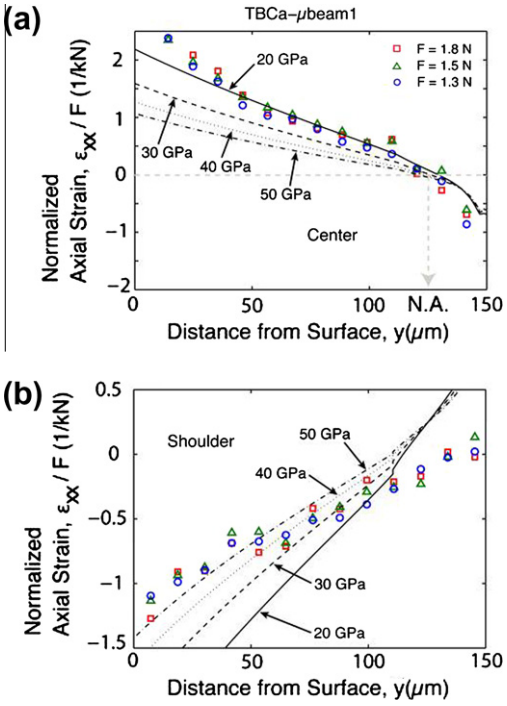

Fig. 7. The normalized experimental strain profile from Fig. 5 compared with a series of FE predictions calculated with a parametric set of in-plane moduli. (a) The strains measured near the center of the microbeam have the TBC in tension and are best modeled with an in-plane TBC modulus of 20 GPa. (b) The TBC strains measured near the shoulder are in compression, were not easily modeled with FE and required an in-plane TBC modulus of greater than 50 GPa.

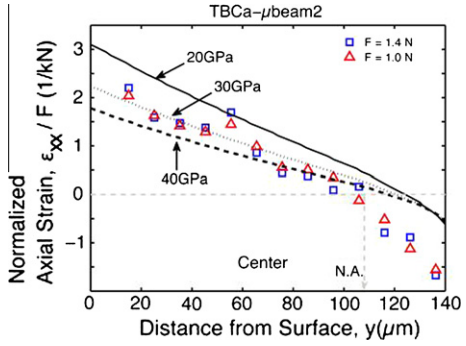

Fig. 8. Experimental data from a different section of the same burner bar compared with FE predictions that were calculated using a series of in-plane TBC moduli. All data were taken near the center of the microbeam with the TBC in tension; the data are best reproduced using a in-plane TBC modulus of 30 GPa.

and loading associated with this microbending experiment dictates that more precise estimates of the strain-dependent modulus be made using detailed FE analysis, which is presented in the next section.

4. Finite-element modeling and interpretation

Finite-element (ABAQUS) simulations of the microbeams used in this study have been employed to account for variations in specimen geometry, loading, overall shape and boundary conditions, and bond coat plasticity. Parametric variations of the in-plane TBC modulus allowed for identification of representative top coat moduli and as well as investigation of the strain and depth dependence of the in-plane TBC modulus. The experimental data presented in Fig. 5 are compared with a series of FE simulations of the microbeam response in Fig. 7. Comparison of the data taken in the center of the microbeam, with the TBC predominantly in tension (Fig. 7a), indicates that the in-plane modulus of the TBC is approximately $E_{TBC} = 20$ GPa, which is comparable with the modulus predicted by the position of the neutral axis (Table 1). By comparison, the FE simulations do not agree as well with the strain distribution measured 150 μm off the shoulder of the specimen. The FE curves based on a in-plane modulus of 50 GPa begin to approach the experimental data, but this value is much higher than measured in the center of the beam. These shoulder measurements were made using a cracked specimen, and strain localization associated with this crack may not have been appropriately captured in the FE simulation. These experiments are also much more sensitive to specimen geometry and the occurrence of plasticity in the shoulder of the specimen. These complications suggest that measurements of the in-plane TBC modulus by the microbeam method are best made with data and simulations obtained in the center of the beam. For this reason, the shoulder measurements were not pursued further, and all of the data presented in the remainder of this study were taken from the center of the microbeams, where the TBC is principally in tension.

The strain dependence of the in-plane modulus E_π was investigated by conducting a series of FE simulations using a simple, linear, representation:

$$\frac{E_{\prod}}{E_0} = \left|1 - \frac{\varepsilon_{xx}}{\varepsilon_0}\right| \quad \left(E_{\prod} \leqslant E_{solid}\right) \tag{2}$$

where E_{solid} is the modulus of the fully dense solid, E_o is the in-plane modulus of the unstrained TBC, and ε_o is the tensile strain at which the modulus vanishes. Incorporation of the strain-dependent modulus resulted in a fanning out of the normalized curves presented in Fig. 5c, in a way that

Table 1
Experimental values of in-plane TBC modulus determined by two methods.

	Width (μm)	h_{na} (μm)	h_{TBC} (μm)	h_{BC} (μm)	E_{BC} (GPa)	E_{TBC} (GPa) from Eq. (1)	E_{TBC} (GPa) from FE
TBC a–microbeam 1	550	120	110	50	155	16	20
TBC a–microbeam 2	550	107	110	40	155	25	30
TBC b–microbeam 1	400	145	150	40	155	15	15–20

was not observed in the experimental data. Moreover, use of the strain-dependent modulus did not result to a fit of the data in Fig. 7a that was better than could be achieve with a strain-invariant modulus. Thus, over the range of stresses and strains imposed in the microbeam experiments, the in-plane modulus of the coatings investigated in this study was deemed to be constant.

The normalized data taken from a different location on the same burner rig bar that was used for the data in Figs. 5 and 7 are shown in Fig. 8. The normalized ε_{xx} strain for this sample (TBC a–microbeam 2) collapses to a single curve for two different loads and the neutral axis for this microbeam was measured to occur at a depth of 107 μm. Combining this neutral axis measurement with the analytical solution in Eq. (1) predicts a slightly higher in-plane TBC modulus (25 GPa) than was obtained in the previous sample. FE curves were calculated using a range of in-plane modulus values, and the curve that best fits the experimental data in the TBC was based on a modulus of 30 GPa (Fig. 8), which agrees with both the analytical analysis and the in-plane modulus obtained on the previous specimen.

The experimental data for a third sample, taken from a different burner rig bar, with a slightly thicker TBC but deposited under nominally identical processing conditions, are presented in Fig. 9. As with the previous samples, the data for three different loads were found to collapse to a common curve when normalized by the applied force. The neutral axis for this sample (TBC b–microbeam 1, measured 80 μm off-center) was observed at a depth of 145 μm, and predictions using Eq. (1) yield an in-plane TBC modulus of 15 GPa. FE analysis of this specimen indicates that the in-plane TBC modulus for this sample lies between 15 and 20 GPa.

EBPVD coats have a columnar microstructure and through-thickness variations in microstructure. Grains that are finest near the substrate and coarsen as the columns grow are commonly observed. This variation in microstructure may be expected to cause a through-thickness

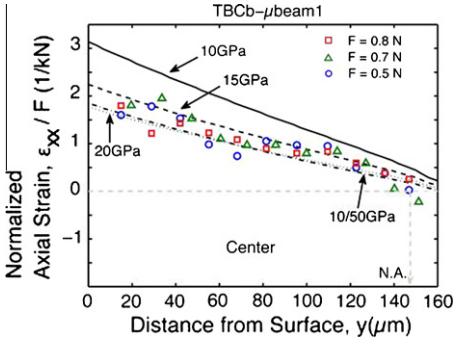

Fig. 9. Experimental data collected from a different burner bar specimen that was deposited with the same commercial process and compared with FE predictions that were calculated using a series of in-plane moduli. All data were taken near the center of the microbeam where the TBC was in tension and the FE data suggest that the in-plane TBC modulus is between 15 and 20 GPa.

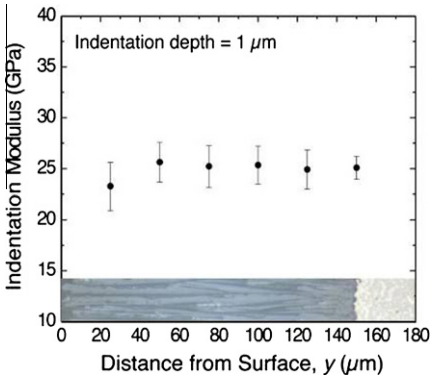

Fig. 10. Nanoindentation measurements of the TBC modulus were obtained on the cross-section of a polished EBPVD 7YSZ TBC and are plotted as a function of distance from the TBC surface. No appreciable variation in modulus with depth was observed.

variation in the in-plane modulus of the TBC. The data presented in Fig. 9 have also been compared with FE simulations conducted with an in-plane modulus that varied linearly through the TBC. Various combinations were tried and the simulation that best fit the experimental data was calculated by assuming that the TBC modulus was 50 GPa at the bottom (near the bond coat) and 10 GPa at the top (near the surface). The result from this simulation (shown in Fig. 9) is almost identical to that obtained by assuming a constant in-plane modulus of 20 GPa, and it is clear that the microbeam experiments are not sufficiently accurate to distinguish between the two. An estimate of the variation in modulus was obtained using nanoindentation (Fig. 10). The modulus values were obtained using a Berkovich indenter, 1 μm deep indents, and unloading data were all approximately 25 GPa and did not appear to vary significantly across the TBC. Due to the large opening angle of the Berkovich tip depth of 1 μm, the indentation diameter was roughly 7 μm. The stress field beneath the indenter translates even further and the elastic response during unloading therefore samples a large volume over several fibers. Due to the strong anisotropy of the Young's modulus, we assume that a large portion of the deformation during unloading is taking place perpendicular to the YSZ fibers. Therefore, the measured Young's modulus mostly resembles the in-plane modulus and can be compared to the beam bending measurements.

5. Discussion

The protocol developed for bilayer microbeams and employed in this study provides a much-needed way of measuring the mechanical behavior of fragile coatings. Demonstrated on cylindrical TBC burner rig specimens, the specimen design is attractive because it allows for testing of ceramic coatings that are too fragile to be handled as free-standing films. The use of DIC provides time-resolved, full-field strain maps, which when combined with FE sim-

ulations provide a reliable measure of the elastic and fracture response of the coating. The incorporation of FE analysis into the test methodology also allows for the application of this protocol to a variety of specimen geometries and sets the stage for the in situ characterization of TBCs deposited on actual turbine aerofoils. Broader use of this methodology to ascertain the importance of external factors (substrate curvature, in-service sintering, foreign deposits, etc.) on the in-plane TBC modulus and resistance to fracture are envisioned.

The proposed protocol has been used to measure the in-plane elastic modulus of a commercially fabricated EBPVD 7YSZ thermal barrier coating, and the results of this exercise are summarized in Table 1. The magnitude of the in-plane TBC modulus was determined to be in the range of 15–30 GPa. These values fall well within the broad range of values previously obtained using compression testing of free-standing cylindrical coatings (10–26 GPa) [3], flexural resonance (10–80 GPa) [2], mechanical spectroscopy (22 GPa) [14] and indentation techniques (60–170 GPa) [15,16]. The in-plane modulus of EBPVD 7YSZ coatings have been reported to depend on the residual stress in the coating, with the highest in-plane modulus being observed in coatings deposited with high compressive stresses [2]. The in-plane modulus for coatings with residual stresses in the range of −25 to +25 MPa were reported to be in the range of 10–30 GPa [2]. Omitting the measurements made using indentation techniques, which induced inherently high compressive stresses, and restricting the other data sets to moderate values of residual stress reduces the overall range of reported literature values for the in-plane modulus of 7YSZ coatings to 10–30 GPa, which is in very good agreement with the values obtained in the current study. This matching is encouraging and shows that the presented methodology seems to work well for TBC material systems. Therefore, in future the methodology will be used to track the changes in elastic properties of as-deposited and in-service parts.

The effect of residual stress on the in-plane modulus of EBPVD 7YSZ TBC deserves further attention. As-deposited 7YSZ contains intercolumnar gaps and intracolumnar porosity, which significantly reduce the in-plane modulus. It is widely believed that as the gaps between the columns open and close upon application of tensile or compressive loads, the number density of contacting sites on the column surfaces varies, resulting in a strain dependence of the in-plane modulus. Measurements made under the application of highly compressive residual stresses appear to support this hypothesis [2]. By contrast, the measurements made in the current study do not; they indicate that the in-plane modulus is invariant with strain. Full interpretation of this data set requires an independent measure of the residual stress state of the TBC.

Residual stresses derived upon cooling from deposition temperatures should lead to compressive stresses in the TBC as the coefficient of thermal expansion for 7YSZ is smaller than for the metallic bond coat and substrate.

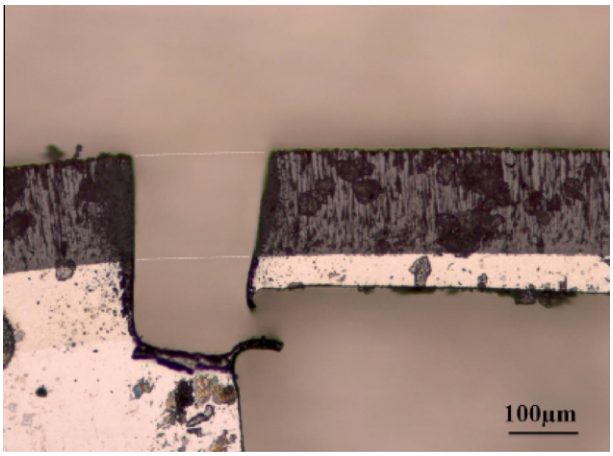

Fig. 11. Cross-sectional optical micrograph of a doubly-end-fixed microbeam that was manufactured by micro-EDM and subsequently cut on one end to produce a free-standing cantilever. The fact that the cantilever did not deflect after cutting has been taken as an indication that the residual stress in these specimens is negligible.

However, removal of the underlying substrate with micro-EDM during the fabrication of the microbeam can be expected to alter the residual stress state. To further explore this issue, a microbeam specimen was sacrificed and used to estimate the residual stresses in the TBC prior to testing. Fig. 11 shows the shoulder of a doubly-end-supported microbeam that has been cut to produce a free-standing cantilever. Residual stresses would be expected to result in deflection of the tip of the bilayer cantilever, but no perceptible displacement of the free end of the cantilever was detected. This has been taken to mean that the residual stresses in the microbeam specimens are relieved during micro-EDM and are negligible. Thus, the stresses in the TBC can be estimated from the elastic strain that is imposed during the microbeam experiments.

The maximum strain to fracture for the microbeams was measured to be $3.5–5.0 \times 10^{-3}$, which when multiplied by an in-plane modulus of 20 GPa indicates that the maximum local tensile stress that a TBC can support would be of the order of 70–100 MPa. In reality, the applied stresses varied with position in the microbeam and were significantly lower than this. It is interesting to note that invariance of the in-plane modulus was measured using the center of the microbeam, where the stresses in the TBC were predominantly tensile. By contrast, the data from the near-shoulder region, where the compressive stresses were dominant, appeared to be much higher and could not be fit with the FE analysis. The most straightforward interpretation of these findings appears to be that the strain dependence of the in-plane TBC modulus is valid in compression but not in tension. We note that the tests reporting strain dependence in the literature were all conducted in compression, owing primarily to the fragile nature of TBC coatings. The physical interpretation of this result appears to be that pores are continually crushed together during compressive loading but once separated do not change their contact area appreciably when loaded in tension.

6. Summary

The protocol presented here allows for the measurement of the in-plane Young's modulus and fracture strain of fragile ceramic coatings and is demonstrated with EBPVD TBCs. Analytical solutions based on elementary beam theory provide reasonable estimates of the in-plane modulus. Comparison of FE simulations with the strain distribution obtained with a three-point microbeam bending experiment, measured by DIC, provide a much more flexible tool for characterizing the elastic and fracture response of the coating. Using of this method, the in-plane modulus of an as-deposited EBPVD 7YSZ TBC was determined to be in the range of $E_{TBC} = 15$–30 GPa in tension. Moreover, the data collected in this study indicate that effect of elastic strain on the in-plane modulus of an EBPVD coating is more significant in compression than it is in tension. The in-plane modulus was found to be invariant with strain in tension. The strain to failure of this coating (by introduction of a through-thickness crack) was observed to be in the range of $\varepsilon_{crit.} = 3.5$–$5 \times 10^{-3}$, which indicates that the TBC can support upwards of 70–100 MPa of stress locally.

References

[1] Stecura S. NASA Tech Mem 78976, N78-31212; 1978.
[2] Johnson C, Ruud J, Bruce R, Wortman D. Surf Coat Technol 1998;108–109:80–5.
[3] Bartsch M, Fuchs U, Xu J. Ceram Eng Sci Proc 2008;28:11–8.
[4] Xiao J, Liu C, Zhao W, Fu W. Mater Sci Forum 2003;423–425:555–60.
[5] Eberl C, Gianola DS, Hemker KH. Exp Mech 2010;50:85–97.
[6] Mercer C, Faulhaber S, Evans A, Darolia R. Acta Mater 2005;53:1029–39.
[7] Peters WH, Ranson WF. Opt Eng 1982;21:427–31.
[8] Chu TC, Ranson WF, Sutton MA, Peters WH. Exp Mech 1985;25:232–44.
[9] Bruck HA, McNeill SR, Sutton MA, Peters WH. Exp Mech 1989;29:261–7.
[10] Eberl C, Thompson RJ, Gianola DS. Free digital image correlation and tracking functions. <http://www.mathworks.com/matlabcentral/fileexchange/12413>.
[11] He MY, Hutchinson JW, Evans AG. J Appl Mech 2011;78:011009-1–011009-5.
[12] Hemker KJ, Mendis BG, Eberl C. Mater Sci Eng A 2008;483:727–30.
[13] Suo Z, Hutchinson JW. Int J Fract 1991;43:1–18.
[14] Gregori G, Lì L, Nychka J, Clarke D. Mater Sci Eng A 2007;466:256–64.
[15] Zhao X, Xiao P. Surf Coat Technol 2006;201:1124–31.
[16] Malzbender J, Steinbrech R. J Mater Res 2003;18:1975–84.